Energy-Gap Dependence of Photoinduced Charge Separation and Subsequent Charge Recombination in 1,4-Phenylene-Bridged Zinc – Free-Base Hybrid Porphyrins

Atsuhiro Osuka,*[a] Go Noya,[a] Seiji Taniguchi,[b] Tadashi Okada,*[b] Yoshinobu Nishimura,[c] Iwao Yamazaki,[c] and Noboru Mataga*[d]

Abstract: A series of 1,4-phenylene-bridged ZP-HP hybrid porphyrins (ZP = zinc porphyrin, HP = free-base porphyrin) **1**–**8ZH** have been prepared in which an electron-donating ZP moiety is kept constant and electron-accepting HP moieties are varied by introducing electron-accepting substituents, so that the energy gap for charge separation, ZP-^{1}HP* $\rightarrow$ZP$^+$-HP$^-$, covers a range of about 0.9 eV in DMF. Here selective excitation at the HP moiety was employed to avoid complication in the determination of electron transfer rates derived from energy transfer, ^{1}ZP*-HP $\rightarrow$ZP-^{1}HP*. Definitive evidence for the electron transfer has been obtained in three solvents (benzene, THF, and DMF) through picosecond–femtosecond transient absorption studies, which have allowed the determination of the rates of the photoinduced charge separation, ZP-^{1}HP* $\rightarrow$ZP$^+$-HP$^-$, and subsequent thermal charge recombination ZP$^+$-HP$^-$ $\rightarrow$ZP-HP. Dyad **1ZH** in THF exhibits a biphasic fluorescence decay that indicates thermal repopulation of the ZP-^{1}HP* from ZP$^+$-HP$^-$; this has been also supported by the transient absorption spectra. On this ground, the energy levels of the ZP$^+$-HP$^-$ ion pairs have been estimated. Similar biphasic fluorescence decay has been observed for **5ZH** in benzene; this allows furhter estimation of the energy level of the ZP$^+$-HP$^-$ ion pairs. The free-energy-gap dependence (energy-gap law) has been probed from the normal to the upper limit region for the rate of the charge separation alone, and only the inverted region for the rate of the charge recombination. It was not possible to reproduce both energy-gap dependencies of the charge separation and the charge recombination assuming common parameter values for the reorganization energy and electronic interaction responsible for the electron transfer with the classical Marcus equation. Although both energy-gap dependencies can be approximately reproduced by means of the simplified semiclassical equation, which takes into consideration the effect of the high-frequency vibrations replaced by one mode of averaged frequency, many features, which include the effects of solvent polarity, electron-tunneling matrix element, and so forth on the energy-gap law, are considerably different from those of the previous studied porphyrin–quinone systems with weaker inter-chromophore electronic interactions.

Keywords: charge recombination · charge separation · kinetics · porphyrinoids · zinc

[a] Prof. A. Osuka, G. Noya
Department of Chemistry, Graduate School of Science
Kyoto University, Kyoto 606-8502, (Japan)
and Core Research for Evolutional Science and Technology (CREST)
of Japan Science and Technology (JST) Corporation (Japan)
Fax: (+81) 75-753-3970
E-mail: osuka@kuchem.kyoto-u.ac.jp

[b] Prof. T. Okada, Dr. S. Taniguchi
Department of Chemistry, Graduate School of Engineering Science
and Research Center for Extreme Materials, Osaka University
Toyonaka 560-8531 (Japan)

[c] Prof. I. Yamazaki, Dr. Y. Nishimura
Department of Chemical Process Engineering
Graduate School of Engineering
Hokkaido University, Sapporo 060-8628 (Japan)

[d] Prof. N. Mataga
Institute for Laser Technology, Utsubo Honmachi, Nishi-ku
Osaka 550-0004 (Japan)

Introduction

Among many factors that control electron transfer (ET) reactions, the free-energy-gap ($-\Delta G$) dependence of the ET rate (energy-gap law) has been most intensively studied with a view to confirm the prediction based on Marcus theory.[1] ET can occur by very weak electronic coupling between a donor and an acceptor, for which the nonadiabatic approximation is valid and the ET rate constant k_{ET} is given by Equation (1),

$$k_{ET} = \frac{2\pi}{\hbar} V^2 \mathrm{FCWD} \quad (1)$$

which treats ET as radiationless transition. In this expression, V is the electronic tunneling matrix element, and FCWD represents the nuclear coordinates as the Franck–Condon weighted density of states.[2] FCWD depends on the energy-

  0947-6539/00/0601-0033 $ 17.50+.50/0

gap, the nuclear vibrational mode relevant to the ET process, the changes of bond lengths and angles of substrates, and the changes of solvation upon ET.

Elucidation of the energy-gap law of the ET rate is quite important in understanding the photoinduced ET events that occur in the photosynthetic reaction center[3] and in the design of effective artificial models that can mimic the photosynthetic charge separation.[4] Equation (1) predicts a nonsymmetrical bell-shaped energy-gap dependence that includes normal, upper limit, and inverted regions, and which, though long controversial, has been confirmed from experiments on donor–acceptor pairs held by protein frameworks[5] and covalent networks of rigid spacers.[6] In those cases, the distance between the donor and acceptor is kept constant, thus circumventing diffusion and making the ET reaction a unimolecular process. In the meantime, it has been also recognized that the energy-gap dependence is not uniform, but depends on the reaction mode.[7] For a donor–acceptor system covalently linked by a rigid steroidal spacer, the bell-shaped dependence has been confirmed for charge-shift reactions (CSH),[6] while only the normal and upper limit regions have been experimentally observed for charge separation reactions (CS) and only the inverted region has been detected for charge recombination reactions (CR).[8–12]

For unlinked donor–acceptor systems in solution, long-standing and quite extensive investigations have been made on the energy-gap law of the excited state ET for luminescent-quenching reactions and also of the back ET process in the production of geminal radical ion pairs.[7, 13–16] In spite of a wide energy-gap range larger than 2 eV, no inverted region has been observed for the CS rate in fluorescence-quenching reactions in strongly polar solvents like acetonitrile.[7, 13–16] In contrast, approximately bell-shaped energy-gap dependencies of the CR reaction rate of loose geminal ion pairs (LIPs) produced by CS in the fluorescence-quenching reaction have been demonstrated.[7, 13, 16] Vigorous experimental and theoretical investigations have been performed to elucidate the underlying reasons for failure in observation of the inverted region in the energy-gap dependencies of k_{CS} and difference between the energy-gap dependencies of k_{CS} and k_{CR}.[7, 13–15]

Because the k_{CS} value for the favorable energy-gap ($-\Delta G_{CS}$) region is masked by the diffusion limit of the reaction, "true k_{CS} values" were estimated by analyzing transient effects in the fluorescence-quenching process for a series of fluorescer–quencher pairs that cover a wide $-\Delta G_{CS}$ range.[16d] Nevertheless, very broad and rather flat k_{CS} versus $-\Delta G_{CS}$ plots were obtained that had no inverted region.[16d] On the basis of detailed examinations,[7, 16b,c,e,f] the most probable explanation for this relation rests on distance distribution between fluorescer and quencher, that is, the increase of average ET distance with increase of the energy gap. In the CS with larger $-\Delta G_{CS}$, a larger solvent reorganization energy λ_s is favorable to keep activation energy small and k_{CS} large, and a larger λ_s also means a large fluorescer–quencher distance at which ET takes place (see Equations (10) and (12) later); this makes the detection of the inverted region even more difficult. A quantitative analysis of the transient effect led to calculation of the time-dependent "CS rate constant, $k_{CS}(t)$" by averaging the distance-dependent $k_{CS}(t)$ with the distribution function $p(r,t)$ obtained by numerically solving the diffusion-reaction equation.[7b,e–g, 16e,f] Moreover, the almost bell-shaped k_{CR} versus $-\Delta G_{CR}$ relationship of the geminal LIPs was reproduced approximately by assuming the same parameter values for calculations and only slight modifications of the initial ionic distance distributions in the product geminal LIPs during CR.[7b,e–g, 16e,f]

Thus, systematic parameter values for the calculations were given at the same time both for the observed k_{CS} versus $-\Delta G_{CS}$ relationship with no clear-cut inverted region and the approximately bell-shaped k_{CR} versus $-\Delta G_{CR}$ relationship of the LIPs. While it seems to be of crucial importance to examine this problem by means of a series of donor–acceptor systems with fixed distance or fixed structure for the final confirmation of the mechanism,[17] there are some other problems related to the energy-gap laws of the photoinduced ET reactions. Namely, non-Marcus type k_{CR} versus $-\Delta G_{CR}$ relationship was found for contact ion pairs (CIPs), which are formed by exciting ground state CT complexes, such as aromatic hydrocarbon complexes of tetracyanobenzene (TCNB), benzene tetracarboxylic acid dianhydride, and tetracyanoethylene (TCNE) in solution.[7a,d,f,g, 15] For these CIPs, exponential energy-gap laws of $k_{CR} = \alpha \exp[-\beta |\Delta G_{CR}|]$ have been observed. Interestingly, the same CIPs adsorbed on porous glass without solvent showed essentially the same energy-gap law; this indicates that the role of solvent reorganization is quite minor.[15e] The observed temperature effects of the adsorbed system strongly suggested the dominant effects of the intramolecular high-frequency quantum modes and also the intracomplex (intermolecular or interionic) vibrational modes in the CR.[15e] These results have been interpreted reasonably well on the basis of the theoretical models of intramolecular radiationless transition in the weak coupling limit.[7d,f,g, 15] A similar mechanism might be involved in the ET processes of linked systems when the interchromophore interactions become sufficiently strong.

In the field of artificial photosynthetic model studies, investigations of photoinduced CS as a function of $-\Delta G$ have been carried out so far mostly with synthetic models that consist of a porphyrin donor linked with quinone or other small organic acceptors.[8–12] These studies have shown the reaction-mode-dependent energy-gap laws are as noted above and kinetic data that are generally consistent with the Marcus theory with reorganization energies of $1 \sim 1.5$ eV in fluid organic solvents. On the other hand, there are only scattered studies on the energy-gap dependence for interporphyrin ET reactions, despite the fact that the initial ET in photosynthesis occurs between two tetrapyrrolic pigments. Gust et al. have reported that the energy-gap dependence for ET in amide-bond-linked TPP-type porphyrin dyads is similar to those of porphyrin–quinones, exhibiting normal and upper limit regions with $\lambda = 1.30$ eV for zinc-porphyrin donor series and $\lambda = 1.17$ eV for free-base donor series in CH_2Cl_2.[11] However, their studies mostly relied on the measurement of fluorescence lifetimes and suffered from difficulty in the division of the large decay rates of the S_1 state of zinc porphyrin into energy transfer and ET processes.

In this paper we report the synthesis of ZP-HP (ZP = zinc porphyrin, HP = free-base porphyrin) dyads **1**–**8ZH** (Fig-

0947-6539/00/0601-0034 $ 17.50+.50/0 *Chem. Eur. J.* **2000**, *6*, No. 1

ure 1) bridged by a 1,4-phenylene spacer and the picosecond fluorescence-lifetime measurements and picosecond–femtosecond time-resolved transient absorption studies by which rates of both photoinduced forward CS (k_{CS}) and thermal

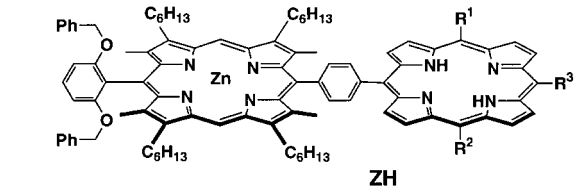

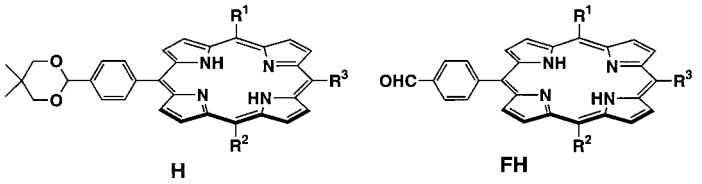

1; $R^1=R^2=H$, $R^3=Ar$

2; $R^1=H$, $R^2=Br$, $R^3=Ar$

3; $R^1=H$, $R^2=H$, $R^3=C_6F_5$

4; $R^1=R^2=Br$, $R^3=Ar$

5; $R^1=R^2=R^3=C_6F_5$

6; $R^1=NO_2$, $R^2=H$, $R^3=C_6F_5$

7; $R^1=R^2=C_3F_7$, $R^3=C_6F_5$

8; $R^1=R^2=NO_2$, $R^3=C_6F_5$

Ar=3,5-di-*tert*-butylphenyl

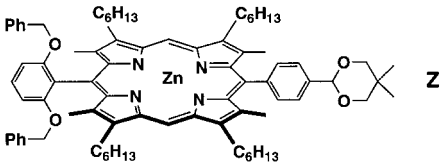

Figure 1. Structures of models compounds studied in this paper, dyads **1**–**8ZH**, reference free-base porphyrins **1**–**9H**, formyl-substituted free-base porphyrins **1**–**8FH**, and reference zinc porphyrin **Z**.

backward CR (k_{CR}) have been determined. In the final part, the energy-gap dependence of k_{CS} and k_{CR} will be discussed. In the present porphyrin dyads, the electron-donating ZP moiety is kept constant and variation of the substituents of the electron-accepting HP moieties allows for a wide variation of the energy gap for charge separation, ZP-^{1}HP* $\rightarrow$ZP$^+$-HP$^-$, and for subsequent thermal charge recombination, ZP$^+$-HP$^-$ $\rightarrow$ZP-HP. Here we employed selective excitation at the HP, thereby avoiding complication derived from the energy transfer ^{1}ZP*-HP $\rightarrow$ZP-^{1}HP*. Even under this restriction, the present models can cover a range of 0.42 eV in benzene, 0.70 eV in THF, and 0.90 eV in DMF for the energy gap for CS of ZP-^{1}HP* $\rightarrow$ZP$^+$-HP$^-$. Since the present ZP-HP dyads are expected to have smaller reorganization energies compared with those in the previous porphyrin–quinone models due to more delocalized nature of HP$^-$, we expected the detection of an inverted region at sufficient energy gap for the CS reactions.

Results and Discussion

Synthesis: Porphyrin dyads **1**–**8ZH** were all prepared by the final cross condensation of 2,6-dibenzyloxybenzadehyde (**9**)[18] and formyl-substituted porphyrins **1**–**8FH** with dipyrrylmethane **10** with aid of trichloroacetic acid;[19] this was followed by oxidation with *p*-chloranil and subsequent partial Zn^{II} ion insertion (Scheme 1). Yields of **1**–**8HH** were 12–29% and yields of the partial metalation were 60–90%. Preparations of **1**–**8FH** were shown in Schemes 2–5. Protected free-base porphyrins **1**–**8H** were used as the reference

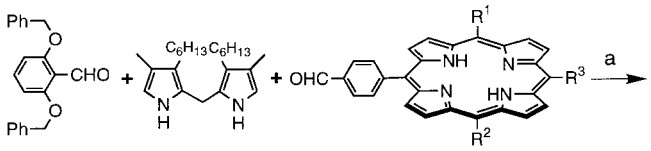

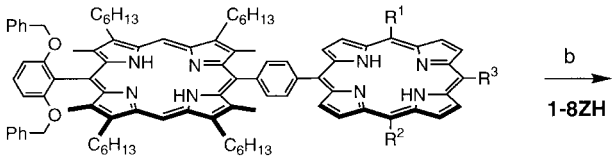

1-8HH

Scheme 1. Synthesis of dyads **1**–**8ZH**. a) i) TFA, CH_2Cl_2, 16 h, RT; ii) *p*-choranil, 8 h, RT. b) $Zn(OAc)_2$/MeOH, CH_2Cl_2, 5 min, RT.

molecules. Compounds **1**–**8H** were hydrolyzed to **1**–**8FH** under acidic conditions (TFA and H_2O, reflux), while **1**–**8FH** were converted to **1**–**8H** upon heating in the presence of neopentyl glycol and *p*-TsOH. Cross condensation of 4-(5,5-dimethyl-1,3-dioxan-2-yl)benzaldehyde (**11**)[18] and 3,5-di-*tert*-butylbenzaldehyde (**13**) with dipyrrylmethane (**12**) with aid of TFA followed by oxidation with *p*-chloranil (Lindsey's conditions)[20] produced three porphyrin products that were separated over a silica gel column to provide **1H** in 18% yield (Scheme 2). Porphyrin **3H** was similarly prepared from the

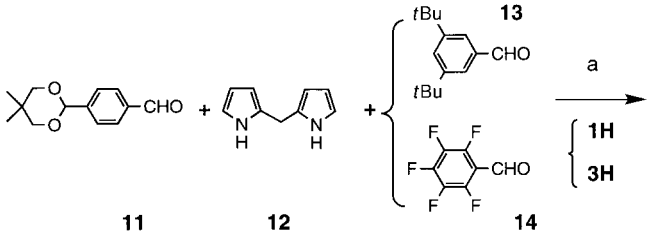

Scheme 2. Synthesis of **1H** and **3H**. a) i) TFA, CH_2Cl_2, 3 h, RT; ii) *p*-choranil, 2 h, RT.

condensation of **11** and pentafluorobenzaldehyde (**14**) with **12** in 14% yield (Scheme 2). *meso*-Brominated porphyrins **2H** and **4H** were prepared by NBS bromination of **1H** in 42 and 14% yields, respectively.[21] Nitration of the zinc-complex of **3H** with $AgNO_2$ and I_2 in $CHCl_3$[22] gave only the mononitrated porphyrin **15** (42% yield), which was converted to

6FH under acidic conditions (Scheme 3). A dinitrated porphyrin was not formed under these condition, but it has been found that the combination of $NaNO_2$ and $(4\text{-}BrC_6H_4)_3NSnCl_5$[23] converts **15** into dinitrated porphyrin **16** (12%), which was hydrolyzed to **8FH** (Scheme 3). TFA-catalyzed condensation of pyrrole with **14** gave pentafluoro-

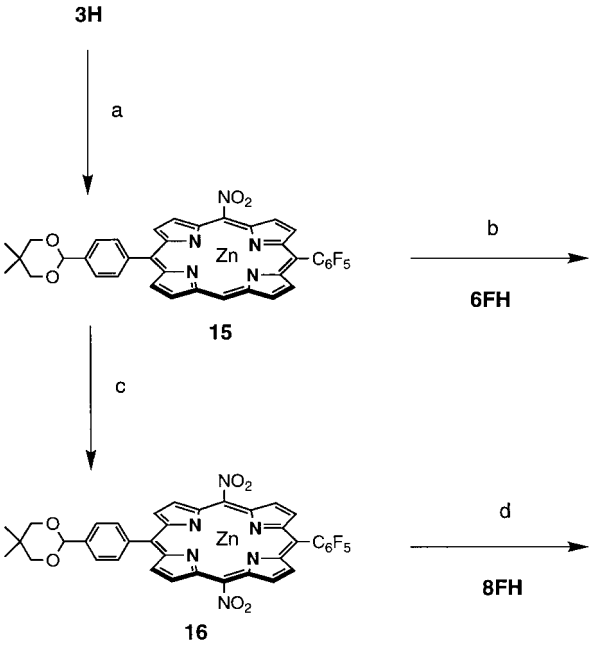

Scheme 3. Synthetic route to **6FH** and **8FH**. a) i) $Zn(OAc)_2$/MeOH, $CHCl_3$, reflux 5 h; ii) $AgNO_2$, I_2, $CHCl_3$, RT, 1 h. b) 6N HCl, $CHCl_3$. c) $(4\text{-}BrPh)_3NSbCl_6$, $CHCl_3$, $NaNO_2$, MeOH, RT, 0.5 h. d) 6N HCl, $CHCl_3$.

phenyl-substituted dipyrrylmethane **17** (85%),[24] which was then treated with 4-methoxycarbonyl-benzaldehyde and **14** to give porphyrin **18** in 16% yield (Scheme 4). Reduction with $LiAlH_4$ and subsequent oxidation with PCC gave **5FH**. Similarly heptafluorobutyraldehyde acetal **20** was treated with pyrrole to give perfluoropropyl-substituted dipyrrylmethane **21** (85%), and the condensation of **11** and **14** with **21** followed by oxidation with DDQ gave porphyrin **7H** (2.8%) (Scheme 5).

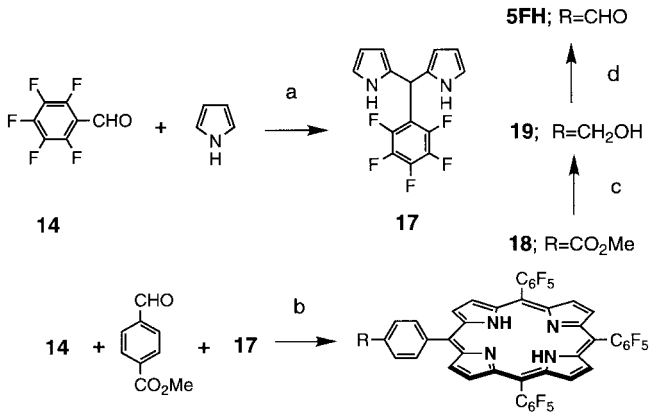

Scheme 4. Synthetic route to **5FH**. a) TFA, 30 min, RT. b) i) BF_3OEt_2, CH_2Cl_2, 3 h, RT; ii) *p*-choranil, 1 h, RT. c) $LiAlH_4$, Et_2O, 0°C, 15 min. d) PCC, CH_3CO_2Na, CH_2Cl_2, RT, 1 h.

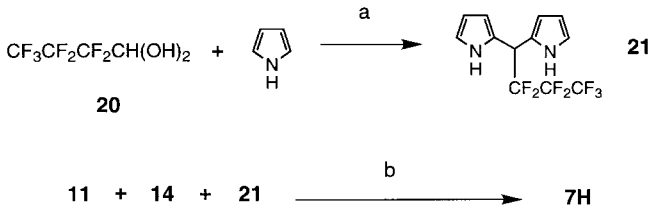

Scheme 5. Synthetic route to **7H**. a) *p*-TsOH, $CHCl_3$, 16 h, reflux. b) i) TFA, CH_2Cl_2, 24 h, RT; ii) DDQ, 5 h, RT.

Optical properties: The absorption spectra of **1**–**8ZH** were almost the sum of those of the respective chromophores, indicating that the electronic interactions in the ground state are negligible (Table 1 and Figure 2). The fluorescence spectrum of **1ZH** taken for excitation at the Soret band in THF (Figure 3) reveals dual emission from ^{1}ZP*-HP and ZP-^{1}HP*. Stronger fluorescence quenching of the ZP indicates the presence of efficient decaying pathways in ^{1}ZP*-HP, either energy transfer to form ZP-^{1}HP* as previously reported in other models[25] or CS to form ZP^+-HP^- or both.[26] The fluorescence intensity of ZP-^{1}HP* depends on the solvent polarity, that is, virtually unquenched in nonpolar benzene, substantially quenched in moderately polar THF (72% quenching), and completely quenched (virtually not detectable by steady-state fluorescence) in polar DMF. Similar trends were observed for the other dyads **2**–**8ZH**. These solvent polarity effects are quite similar to the previous porphyrin-chlorin dyads,[26] which suggests CS between the ^{1}HP* and ZP that will be verified later on the ground of the transient absorption data.

Electrochemical studies and estimation of energy level: In this paper we are only concerned with the free-energy-gap dependence for the CS, ZP-^{1}HP* $\rightarrow ZP^+$-HP^-, and for the subsequent thermal backward CR, ZP^+-HP^- $\rightarrow$ZP-HP. To estimate the free-energy gaps of these two processes, we need to know the energies of ^{1}HP* and ZP^+-HP^- state. The

Table 1. Absorption and fluorescence data of **1**–**8ZH** in THF.

	Soret [nm]		Q-bands [nm]						Fluorescence bands [nm]	
1ZH	406	423	502	544	576	633			634	697
2ZH	414	426	483	513	548	586	647		647	713
3ZH	403	423	499	532	573	627			628	708
4ZH	416	431	487	523	553	585	601	660	665	734
5ZH	426		508	547	584	640			642	708
6ZH	425		507	547	581	635			643	703
7ZH	424		509	546	586	641			644	712
8ZH	426		510	548	584	646			660	715

0947-6539/00/0601-0036 $ 17.50+.50/0 *Chem. Eur. J.* **2000**, *6*, No. 1

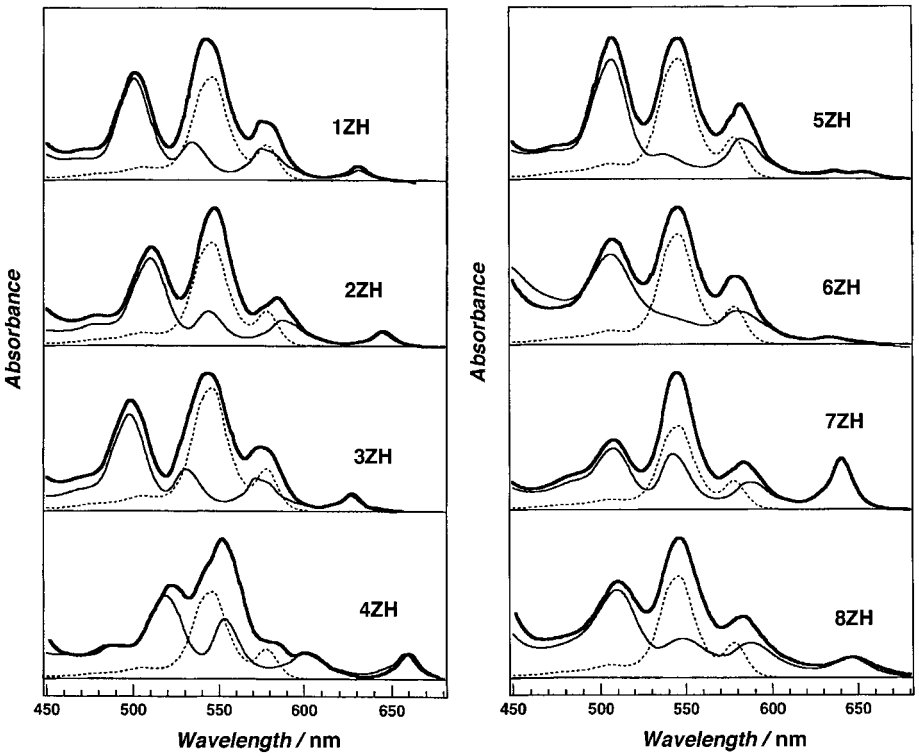

Figure 2. Absorption spectra of **1**–**8ZH** in the Q-band-region; **ZH** (——), **H** (——), and **Z** (- - - -).

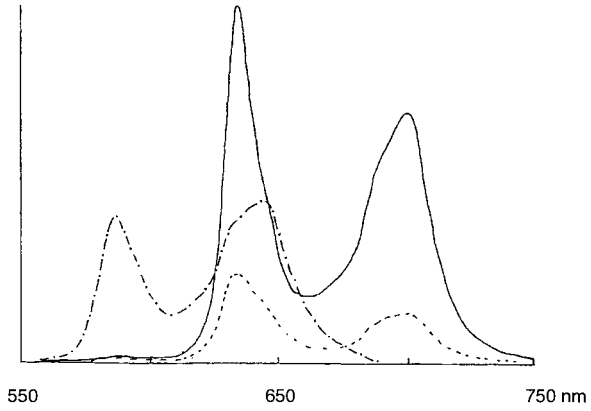

Figure 3. Steady-state fluorescence spectra of **1ZH** (- - - -), **1H** (——), and **Z** (•–•–) in THF taken for excitation at the respective Soret bands.

energies of ^{1}HP* were determined on the basis of the fluorescence and absorption (0,0) bands (Table 2). The energy levels of ZP$^+$-HP$^-$ in DMF are estimated as a simple sum of the one-electron oxidation potential of ZP and corresponding one-electron reduction potential of HP. The energy levels in THF and benzene were estimated by Equations (8) and (9) (see later) by using a correction term (ΔG_s), which was obtained from analysis of biphasic fluorescence decay by Equations (3)–(7) (see later) on the assumption of the thermal repopulation of the singlet-excited state from the ion-pair state. Details will be discussed below.

Determinations of rate constants and energy gaps for CS and CR reactions by means of the fluorescence dynamics studies and time-resolved transient absorption measurements: The fluorescence lifetimes were measured in benzene, THF, and DMF by the single-photon counting technique. In all cases, the fluorescence decays at 700 nm, at which only the HP moieties emit, were measured for excitation at 630 nm, at which the ZP moiety has no absorption and the HP moieties have some absorbance. Coincidentally, **1ZH** exhibits three typical fluorescence decays in benzene, THF, and DMF that suggest the reaction schemes shown in Scheme 6a–c, respectively. Thus we start the discussion of the fluorescence behaviors of **1ZH**. In nonpolar benzene solution, the fluorescence intensity of **1ZH** was the same as that of **1H**, and the fluorescence decay curve has been fit with a single exponential function with $\tau = 9.81$ ns, which is nearly the same as that of **1H** ($\tau_0 = 10.0$ ns). Thus, we concluded no CS (Scheme 6a). In polar DMF solution, the

Table 2. Excitation energy to ^{1}HP* ($E(S_1)$) and energy gaps for the CS and the CR ($-\Delta G_{CS}$ and $-\Delta G_{CR}$).[a,b]

	$E(S_1)$ [eV]	benzene		THF		DMF	
		$-\Delta G_{CS}$ [eV]	$-\Delta G_{CR}$ [eV]	$-\Delta G_{CS}$ [eV]	$-\Delta G_{CR}$ [eV]	$-\Delta G_{CS}$ [eV]	$-\Delta G_{CR}$ [eV]
1ZH	1.96	−0.29	2.25	−0.01	1.97	0.19	1.77
2ZH	1.92	−0.18	2.10	0.10	1.82	0.30	1.62
3ZH	1.98	−0.17	2.15	0.11	1.87	0.31	1.67
4ZH	1.87	−0.14	2.01	0.14	1.73	0.34	1.53
5ZH	1.93	0.01	1.92	0.29	1.64	0.49	1.44
6ZH	1.94	0.16	1.78	0.44	1.50	0.64	1.30
7ZH	1.93	0.26	1.67	0.54	1.39	0.74	1.19
8ZH	1.90	0.42	1.48	0.70	1.20	0.90	1.00

[a] The energy levels of the excited states were determined on the basis of the corresponding fluorescence and absorption (0,0) bands. The energy levels of the ZP$^+$-HP$^-$ states in DMF were a simple sum of the electrochemical redox potential of the respective chromophores; the one-electron oxidation potential of ZP is 0.17 V, and the one-electron reduction potentials of HP are as follows; **1H**, −1.60 V; **2H**, −1.45 V; **3H**, −1.50 V; **4H**, −1.36 V; **5H**, −1.27 V; **6H**, −1.13 V; **7H**, −1.02 V; **8H**, −0.83 V, vs. ferrocene/ferrocenium ion. [b] Energy gaps ($-\Delta G_{CS}$ and $-\Delta G_{CR}$) in benzene and THF were estimated by Equations (8) and (9). The correction terms (ΔG_s) were estimated on the basis of the double exponential decays of **1ZH** in THF and **5ZH** in benzene to be 0.20 eV in THF and 0.48 eV in benzene.

  0947-6539/00/0601-0037 $ 17.50+.50/0

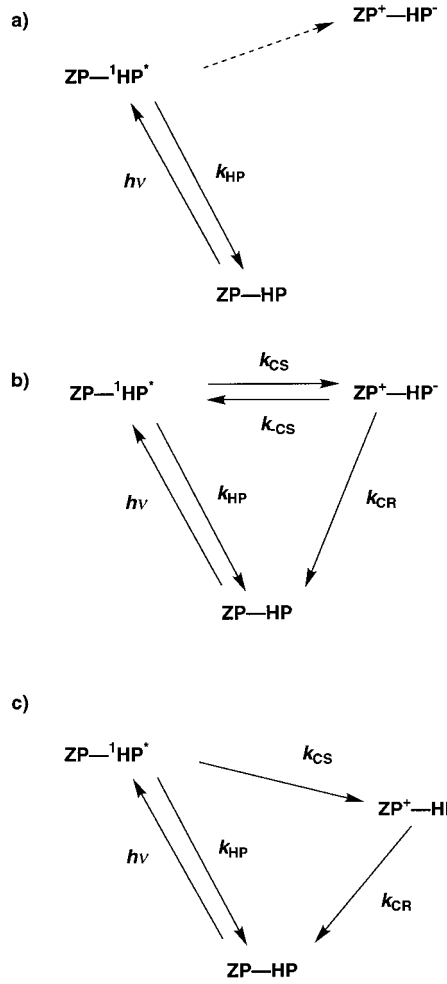

Scheme 6. Reaction scheme for dyads; a) no CS with negative $-\Delta G_{CS}$, b) reversible CS with small $-\Delta G_{CS}$, and c) irreversible CS with large $-\Delta G_{CS}$.

fluorescence was significantly quenched (virtually undetectable by steady-state fluorescence), and the fluorescence decay can be fit by a biexpotential function with a 41 ps lifetime component whose pre-exponential factor was larger than 98%, thus indicating practically a single exponential function. The minor lifetime component may be interpreted in terms of adventitious impurities. These results are consistent with the reaction shown in Scheme 6c, for which the rates of charge separation, k_{CS}, are calculated by Equation (2).

$$k_{CS} = \frac{1}{\tau} - \frac{1}{\tau_0} \tag{2}$$

In Equation (2) τ and τ_0 are the fluorescence lifetimes of ZP-^{1}HP* in **1ZH** and that (11.0 ns) of the corresponding reference free-base porphyrin **1H**, respectively. Equation (2) gives $k_{CS} = 2.5 \times 10^{10}\ s^{-1}$ for **1ZH** in DMF.

The fluorescence of **1ZH** in THF could be only fit with a biexponential function with time constants of 125 ps (33%) and 2460 ps (67%). This biexponential decay indicates the reaction shown in Scheme 6b. This reaction scheme is possible when the energy levels of ZP-^{1}HP* and ZP$^+$-HP$^-$ are close to each other.[8c, 9, 10a, 11c, 26] Assuming this thermal repopulation of ZP-^{1}HP* from ZP$^+$-HP$^-$, k_{CS}, k_{-CS}, and k_{CR} have been calculated according to the well-established procedure [Eqs. (3)–(7)].

$$[ZP - {}^1HP^*] = C_1 e^{-\alpha t} + C_2 e^{-\beta t} \tag{3}$$

$$\alpha = \frac{1}{2}\left(k_{CS} + k_{-CS} + k_{HP} + k_{CR} + \sqrt{(-k_{CS} + k_{-CS} - k_{HP} + k_{CR})^2 + 4k_{CS}k_{-CS}}\right) \tag{4}$$

$$\beta = \frac{1}{2}\left(k_{CS} + k_{-CS} + k_{HP} + k_{CR} - \sqrt{(-k_{CS} + k_{-CS} - k_{HP} + k_{CR})^2 + 4k_{CS}k_{-CS}}\right) \tag{5}$$

$$C_1 = \frac{k_{HP} + k_{CS} - \beta}{\alpha - \beta} \tag{6}$$

$$C_2 = \frac{\alpha - k_{HP} - k_{CS}}{\alpha - \beta} \tag{7}$$

In the above equations k_{CS}, k_{-CS}, k_{HP}, and k_{CR} are defined in Scheme 6b and C_1, C_2, α and β are the experimental values that were determined from the fluorescence decay analysis. Through this analysis with $k_{HP} = 1.0 \times 10^8\ s^{-1}$, the values of k_{CS}, k_{-CS}, and k_{CR} are calculated to be 2.8×10^9, 5.4×10^9, and $9.6 \times 10^8\ s^{-1}$, respectively. On the basis of the relationship $-\Delta G_{CS} = RT\ln(k_{CS}/k_{-CS})$, in which $-\Delta G_{CS}$ is the energy gap for CS, ZP-^{1}HP* $\rightarrow$ZP$^+$-HP$^-$, the energy level of ZP$^+$-HP$^-$ is calculated to be 13 meV higher than that of ZP-^{1}HP*. This result is quite informative on the energy level of the ZP$^+$-HP$^-$, since the apparent relationships of Equations (8) and (9) allow us to estimate the energy levels of ZP$^+$-HP$^-$ for the other **2**–**8ZH** in THF. In Equations (8) and (9), $-\Delta G_{CR}$ is the energy gap for the CR, ZP$^+$-HP$^-$ $\rightarrow$ZP-HP, $E(S_1)$ is the excitation energy of ZP-^{1}HP*, E_{OX} and E_{RED} are the one-electron oxidation and reduction potentials of the ZP and the HP, respectively, measured in DMF, and ΔG_S is the correction term which includes the effects of the solvent polarity and the Coulombic energy between the ZP$^+$ and the HP$^-$.

$$-\Delta G_{CS} = E(S_1) + \Delta G_{CR} \tag{8}$$

$$-\Delta G_{CR} = E_{OX} - E_{RED} + \Delta G_S \tag{9}$$

In the particular case of **1ZH**, $-\Delta G_{CR} = \Delta G_{CS} + E(S_1) = 0.01 + 1.96 = 1.97$ eV and $E_{OX} - E_{RED} = 0.17 - (-1.60) = 1.77$ eV, and thus ΔG_S is estimated to be 0.20 eV. With this correction term ($\Delta G_s = 0.20$ eV), the energy levels of the ZP$^+$-HP$^-$ in THF have been estimated (Table 2). Fortunately, similar biphasic fluorescence decay behavior was also observed for **5ZH** in benzene. By following essentially the same procedure and by using $k_{HP} = 1.0 \times 10^8\ s^{-1}$, the values of k_{CS}, k_{-CS}, and k_{CR} were determined to be 4.0×10^{10}, 2.7×10^{10}, and $9.6 \times 10^8\ s^{-1}$, respectively, which in turn leads to the placement of the ZP$^+$-HP$^-$, by 10 meV, below the ZP-^{1}HP* state for **5ZH** in benzene. These results led to $\Delta G_s = 0.48$ eV, which was conveniently used in the estimation of the energy level of the ZP$^+$-HP$^-$ state in benzene (Table 2).

In benzene, the fluorescence of dyads **1**–**4ZH** are not quenched and display the single exponential decay with lifetimes that are almost the same as those of the reference

0947-6539/00/0601-0038 $ 17.50+.50/0 Chem. Eur. J. 2000, 6, No. 1

1–**4H**; this indicates the endothermic nature of ZP-^{1}HP* →ZP$^+$-HP$^-$ process (Scheme 6a). The fluorescence of **6**–**8ZH** display practically the single exponential decay with short time constants, which suggests the reaction scheme in Scheme 6c. The k_{CS} values can be calculated by Equation (2) with these fluorescence lifetimes. Dyads **2**–**7ZH** in THF and **1**–**5ZH** in DMF exhibit practically the single exponential decay, although the inclusion of weak longer-lived components accounting for impurity fluorescence is necessary in many cases. The k_{CS} values can be calculated also by Equation (2). However, it should be noted here that the time resolution of the fluorescence measurements for **5**–**8ZH** in THF and **1**–**8ZH** in DMF are not sufficient for the accurate determination of the rate constants. In these cases, we have resorted to the femtosecond time-resolved transient absorption measurements. In summary the change in fluorescence behavior from unquenched to biexponential, and to strongly quenched monoexponential decay can be correlated the energy gap of CS; the ET reaction schemes in Schemes 6a–c provide a satisfactory interpretation of these trends.

Transient absorption studies: In Figure 4, picosecond transient absorption spectra of **1**–**8ZH** in THF taken for excitation at 632 nm are displayed. The delay times are indicated in the Figure. In all cases, we can observe clearly the characteristic absorption bands due to ZP$^+$ at 650–680 nm, those due to HP$^-$ in the 800–900 nm region and near 450 nm depending on the nature of the substituents in HP, and also bleaching due to the depletion of ZP ground state at 545 nm. Thus the formation of ZP$^+$-HP$^-$ state has been unambiguously confirmed. Figures 5a and 5b show the picosecond time-resolved transient absorption spectra of **3ZH** and **1ZH**, respectively,

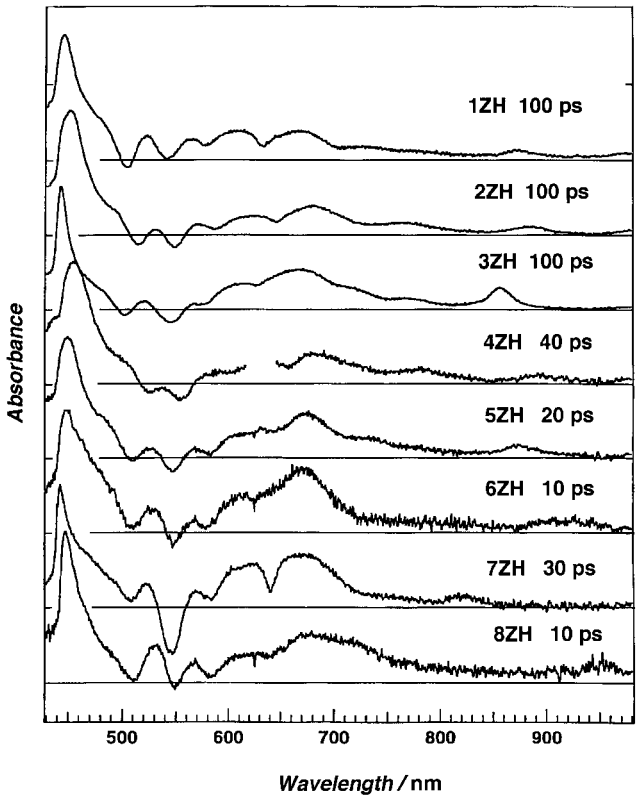

Figure 4. Transient absorption spectra of **1**–**8ZH** taken for excitation at 630 nm in THF. Each diagram represents the spectrum of ZP$^+$-HP$^-$ state. Indicated times in the spectra are delay time after laser excitation.

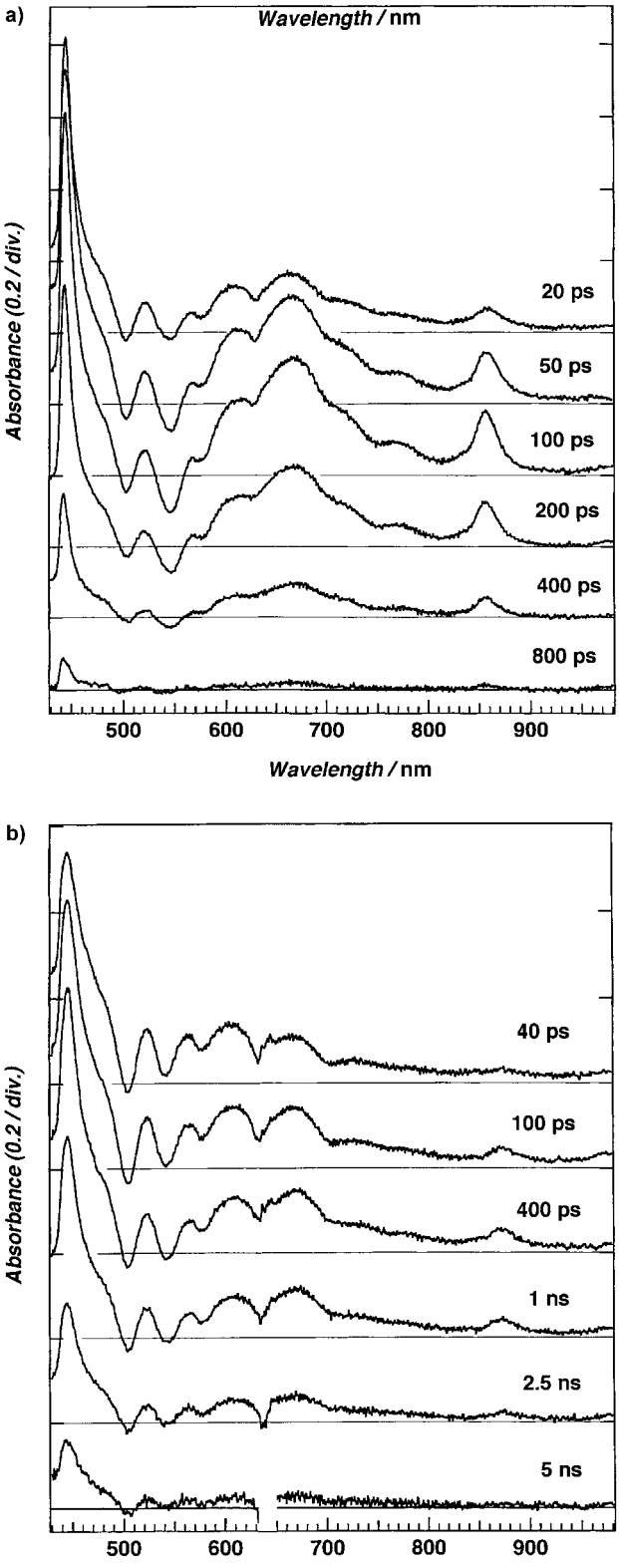

Figure 5. Picosecond transient absorption spectra taken for excitation at 630 nm in THF; a) **3ZH** and b) **1ZH**.

  0947-6539/00/0601-0039 $ 17.50+.50/0

taken for excitation at 630 nm in THF. Excitation at 630 nm enables selective excitation at the HP in the both compounds. These two cases represent irreversible ET (Scheme 6c) and reversible ET (Scheme 6b), respectively, in line with the analysis of the fluorescence-lifetime measurement. In the case of **3ZH** (Figure 5a), immediately after laser excitation the absorption bands at 670 and 857 nm began to appear. On the basis of the relevant reference spectra these bands are assigned to ZP^+ and HP^-, respectively. A sharp absorption band at 445 nm was also assigned to HP^-. At 800 ps delay time, no appreciable amount of the transient absorption species remains; this indicates that an ET cycle that involves the photoinduced CS and subsequent CR are nearly quantitatively completed within 800 ps. In Figure 6, the absorbance

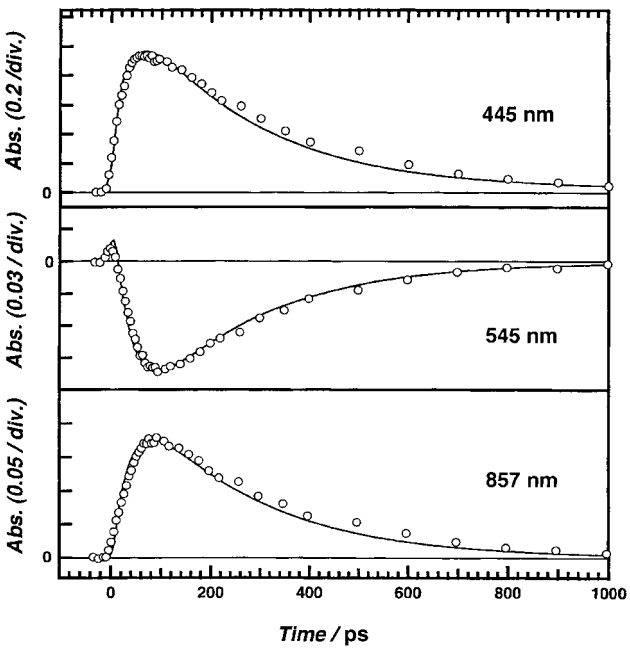

Figure 6. Observed and simulated time profiles of the transient absorbance of **3ZH** in THF at 445, 545, and 875 nm.

rise and decay observed at 445 and 857 nm due to the formation and decay of the ET state, and the bleaching and recovery at 545 nm due to the depletion and recovery of the ZP ground state are indicated. These absorbance changes can be reproduced by biexponential functions with the same rise and decay time constants in accrodance with Scheme 6c. The solid lines in the figures are calculated with the biexponential function. The rise-time constant (35 ps) of ZP^+-HP^- nearly agrees with the fluorescence lifetime (28 ps) of ZP-^{1}HP*. The decay-time constant (240 ps) of ZP^+-HP^- allows us to determine the k_{CR} value. Therefore, on the basis of the ps-time-resloved transient absorption data, k_{CS} and k_{CR} have been determined to be 2.8×10^{10} and $4.2 \times 10^9\ s^{-1}$, respectively.

In the case of **1ZH** in THF, the formation of the ZP^+-HP^- is also evident (Figure 4b). A characteristic band due to the HP^- was observed at 880 nm and a substantial absorbance due to ZP^+ was observed at 670 nm. These bands appear with $\tau =$ 90 ps. Since the lifetime of the reference ^{1}HP* is about 10 ns, the charge separation should be quantitative. The amount of the ZP^+-HP^-, however, was found to be quite small, indicating its fast depletion. Other related models with similar energy gaps are known to undergo much slower CR to the ground state.[26b] Thus reversible ET reactions ZP-^{1}HP* $\rightleftharpoons$ ZP^+-HP^- as shown in Scheme 6b emerge as a possible mechanism. Judging from the spectral shape at 400 – 500 nm at 5 ns delay time, we have to consider the formation of ^{3}HP*. It is plausible that this triplet state is slowly formed from the corresponding ^{1}HP* state, in line with its biexponential fluorescence decay. Time-dependent changes of transient absorbance of **1ZH** at several wavelengths are shown in Figure 7. In this case, from the analysis of the biphasic fluorescence decay dynamics, k_{CS}, k_{-CS}, and k_{CR} are already

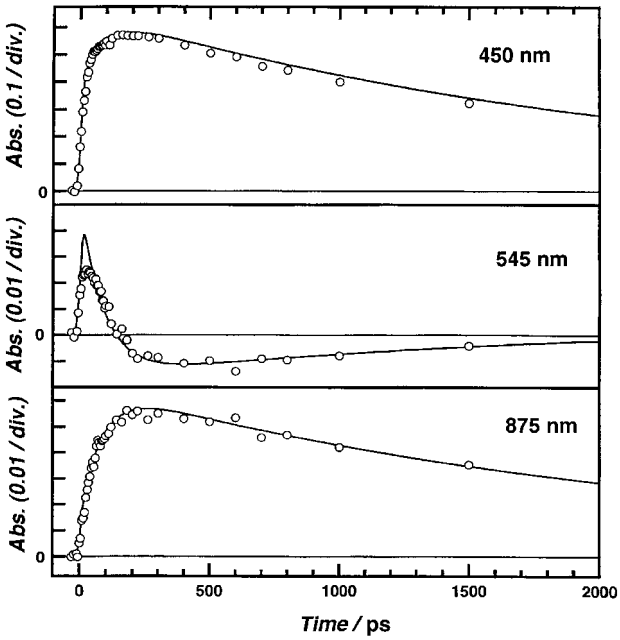

Figure 7. Observed and simulated time profiles of the transient absorbance of **1ZH** in THF at 450, 545, and 875 nm.

determined to be $2.8 \times 10^9\ s^{-1}$, $5.4 \times 10^9\ s^{-1}$, and $9.6 \times 10^8\ s^{-1}$, respectively. By means of Equations (3)-(7) based on Scheme 6b and appropriate values for the difference absorption coefficients of S_1, T_1, and IP states, the time profiles of the transient absorbance have been simulated in a manner similar to those described in the previous report on the porphyrin – quinone dyad system.[9a] The calculated biexponential time profiles of transient absorbances that are indicated by solid curves in the figure nicely reproduce the experimental results, indicating the validity of these treatment. Similar transient spectral changes that support the reaction scheme shown in Scheme 6b are also observed for **5ZH** in benzene (not shown). The rate constants for CS (ZP-^{1}HP* $\rightarrow$ ZP^+-HP^-) and for CR (ZP^+-HP^- $\rightarrow$ ZP-HP), obtained as described, are collected in Table 3.

Free-energy-gap dependencies of k_{CS} and k_{CR}: Usually the numerical analysis of the rate data is frequently undertaken in the framework of nonadiabatic electron transfer theory, where it is assumed that the intra-chromophore high-fre-

0947-6539/00/0601-0040 $ 17.50+.50/0 *Chem. Eur. J.* **2000**, *6*, No. 1

Table 3. Rate constants for CS (ZP-^{1}HP* $\rightarrow$ZP$^+$-HP$^-$) and for CR (ZP$^+$-HP$^-$ $\rightarrow$ZP-HP).

	benzene		THF		DMF	
	k_{CS} [s^{-1}]	k_{CR} [s^{-1}]	k_{CS} [s^{-1}]	k_{CR} [s^{-1}]	k_{CS} [s^{-1}]	k_{CR} [s^{-1}]
1ZH	no CS	–	$2.8\pm0.2\times10^{9}$	$9.6\pm2.3\times10^{8}$	$7.1\pm0.6\times10^{10}$	$1.7\pm0.3\times10^{10}$
2ZH	no CS	–	$1.7\pm0.5\times10^{10}$	4.2 ± 0.4 x10^{9}	$2.1\pm0.2\times10^{11}$	$2.6\pm0.5\times10^{10}$
3ZH	no CS	–	$2.8\pm0.7\times10^{10}$	$4.2\pm0.4\times10^{9}$	$4.3\pm0.5\times10^{11}$	$3.6\pm0.3\times10^{10}$
4ZH	no CS	–	$9.0\pm5.2\times10^{9}$	$9.1\pm2.0\times10^{9}$	$3.1\pm2.0\times10^{11}$	$6.7\pm0.4\times10^{10}$
5ZH	$4.0\pm2.6\times10^{10}$	$9.6\pm8.7\times10^{8}$	$6.7\pm4.4\times10^{10}$	$2.0\pm0.2\times10^{10}$	$5.9\pm2.4\times10^{11}$	$1.1\pm0.2\times10^{11}$
6ZH	$8.1\pm1.8\times10^{10}$	$6.3\pm0.5\times10^{8}$	$7.4\pm1.8\times10^{11}$	$7.7\pm0.6\times10^{10}$	$9.1\pm2.0\times10^{11}$	$3.3\pm0.3\times10^{11}$
7ZH	$7.1\pm1.2\times10^{10}$	$1.1\pm0.1\times10^{8}$	$1.0\pm0.25\times10^{12}$	$6.3\pm2.1\times10^{10}$	$1.3\pm0.2\times10^{12}$	$2.8\pm0.5\times10^{11}$
8ZH	$1.2\pm0.2\times10^{11}$	$1.0\pm0.1\times10^{10}$	$1.14\pm0.2\times10^{12}$	$3.5\pm2.1\times10^{11}$	$1.3\pm0.3\times10^{12}$	$5.9\pm1.5\times10^{11}$

quency vibrations can be replaced by one mode with an averaged frequency and the solvent can be treated as a dielectric continuum, this leads to the well-known expression in Equation (10).

$$k_{ET}=\sqrt{\frac{\pi}{\hbar^2\lambda_s k_b T}}|V|^2\sum_{n}^{\infty}(e^{-S}S^n/n!)\exp\left(-\frac{(\lambda_s+\Delta G+n\hbar\langle\omega\rangle)^2}{4\lambda_s k_b T}\right) \quad (10)$$

$$S=\frac{\lambda_V}{\hbar\langle\omega\rangle} \quad (11)$$

$$\lambda s=\varepsilon^2\left(\frac{1}{2r_A}+\frac{1}{2r_D}-\frac{1}{R}\right)\left(\frac{1}{n^2}-\frac{1}{\varepsilon}\right) \quad (12)$$

In Equation (10) $S=\lambda_v/\hbar\langle\omega\rangle$ is the electron-vibration coupling constant, λ_v is the reorganization energy associated with the averaged angular frequency $\langle\omega\rangle$ and λ_s is the solvent reorganization energy. λ_s is given by Equation (12) according to the classical treatment by Marcus. Although these sort of equations have been rather widely used, it should be noted that its validity is not necessarily warranted particularly in the quantitative analyses of the actual experimental results.

As discussed already to some extent in the Introduction, when the donor–acceptor interaction becomes sufficiently strong, the energy-gap dependence of the CR rate constant of the IP state is drastically changed from the so-called bell-shaped parabolic one to the linear (exponential) one.[7a,d,f,g, 15] In CR, the intramolecular high-frequency quantum modes play important roles[15e] and its ET process can be interpreted on the basis of the theory of intramolecular radiationless transition (internal conversion) in the weak coupling limit.[7, 15] When the donor–acceptor interaction becomes sufficiently strong, the nonadiabatic ET mechanism might become less reliable at favorable energy-gap region for ET and a solvent-controlled ET process in adiabatic regime might take place at the upper limit region of energy-gap dependence of the ET reaction. Such possibilities may not be precluded from the present investigations on ZP-HP systems, since the interchromophore interactions are certainly stronger than the porphyrin–quinone-linked system studied previously.[9a]

Figures 8a–c show semilogarithmic plots of k_{CS} and k_{CR} against $-\Delta G_{CS}$ and $-\Delta G_{CR}$ for **1**–**8ZH** and their simulations by means of Equation (10) in benzene, THF, and DMF, respectively. We have employed a value of 1500 cm^{-1} for $\langle\omega\rangle$ on the basis of the porphyrin macrocycle C=C double-bond frequency and thus used 0.15 eV for $\hbar\langle\omega\rangle$ in all cases. First we determined other parameters from the best fit in the case of THF solution at $T=295$ K, where the most satisfactory

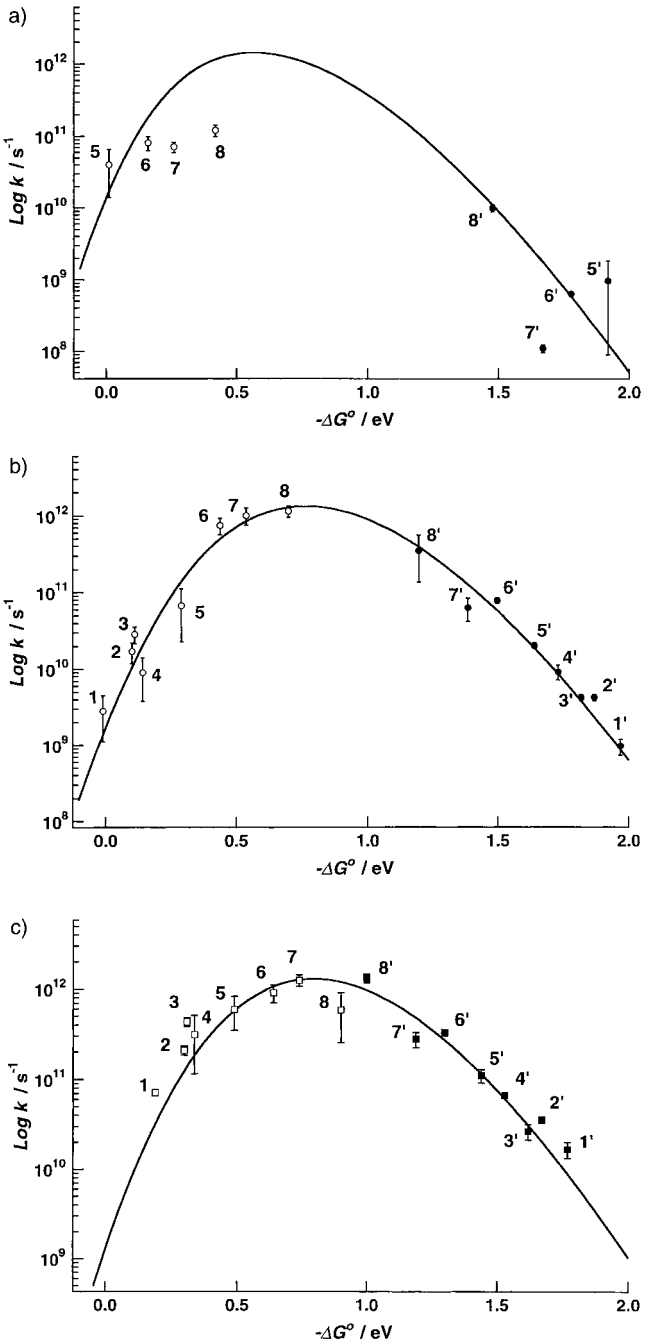

Figure 8. Energy gap dependence of k_{CS} (○ or □) and k_{CR} (● or ■) for **1**–**8ZH** in a) benzene, b) THF, and c) DMF. The curves were calculated by means of Equation (10), with common parameters $T=295$ K, $\lambda_v=0.27$ eV, $V=9.4$ meV, $\hbar\langle\omega\rangle=0.15$ eV, and $\lambda_s=0.35$ eV in benzene, 0.55 eV in THF, and 0.57 eV in DMF.

simulation was possible with $\lambda_s = 0.55$ eV, $\lambda_v = 0.27$ eV, and $V = 9.4$ meV (76 cm^{-1}) (Figure 8b). This λ_s value was coincidentally the same as that calculated with Equation (12) by using reasonable values for the effective radius ($r_D = r_A =$ 5.5 Å, $R = 12.8$ Å). Simulation of the results in benzene and DMF was carried out by adjusting only the λ_s value with other parameters fixed; this lead to $\lambda_s = 0.35$ eV for benzene and $\lambda_s = 0.57$ eV for DMF. For benzene, plots of k_{CS} and k_{CR} values are very limited and rather scattered probably due to some unknown specific solute–solvent interactions, but the simulation curve in Figure 8a obtained by adjusting only λ_s to smaller value corresponds reasonably well to the energy-gap dependence covering whole energy-gap regions including CS and CR. Although the λ_s value in benzene is smaller than those in THF and DMF, it is much larger than that ($\sim$0 eV) calculated by means of Equation (12). Similar results were also observed for the porphyrin–quinone-linked systems.[9a] Equation (12) was derived under the assumption that the simple linear response for the polarization of solvent is applicable in the solute–solvent interactions and the solvent can be regarded as the dielectric continuum. The present and previous results[9a] indicate that the actual interactions between the solute and the solvent in the ET processes are more complex and include effects of some nonlinear solute–solvent interactions and discrete molecular structures of the solution. Recent theoretical treatments on the energetics of ET reactions in solution based on such molecular theories of solution structures seem to agree with the above experimental results of λ_s values.[27]

In contrast to the relatively large λ_s value in benzene, those in THF and DMF are rather small and the difference of λ_s between THF and DMF is also small. These results are considerably different from the solvent polarity dependencies of λ_s in the case of the porphyrin–quinone dyads,[9a] for which λ_s increases more clearly upon increase of solvent polarity. Presumably, the smaller solvent reorganization energy of present models may be ascribed to the fact that both chromophores are porphyrin macrocycles in which the positive and negative charges are well delocalized over a wide range and the two macrocycles are held at very short distance, leading to the weaker interactions with polar solvents.

The tunneling-matrix element of $V = 9.4$ meV determined by the simulation with Equation (10) is considerably larger than the value of $\sim$6 meV reported for the Gust and Moore's porphyrin dyads[11b] and the value of $V = 3.8$ meV in the case of the porphyrin–quinone system;[9a] this seems to reflect considerably stronger inter-chromophore interactions in the present system. Nevertheless, the fact that the simulations of the observed ET rate constants, including both k_{CS} and k_{CR}, over a wide energy-gap range, calculated by means of Equation (10), seem to show satisfactory results in Figure 8; this presumably indicates that the nonadiabatic mechanism is still applicable as a whole. It is noteworthy that the simulations of the experimental results as shown in Figures 8a–c covering the wide energy-gap range are not possible when the classical Marcus equation [Eq. (13), in where $\lambda = \lambda_s + \lambda_v$, V is the tunneling matrix element][28] is applied (not shown).

$$k_{ET} = \sqrt{\frac{\pi}{\hbar \lambda_s k_\beta T}} |V|^2 \exp\left(-\frac{(\lambda + \Delta G)^2}{4 \lambda_s k_\beta T}\right) \quad (13)$$

This means that Equation (13) can approximately reproduce the energy-gap dependencies of only the CS reaction (k_{CS}) or the CR reaction (k_{CR}), but cannot reproduce the k_{ET} versus $-\Delta G_{ET}$ relationship that includes both the reactions. Particularly for k_{CR} at large $-\Delta G$ values (1–2 eV), the observed rate constants are higher than the simulated curves in general, suggesting the crucial importance of the intrachromophore high-frequency vibrational modes for the ET in this energy-gap region. It is to be noted that the CS reactions in THF and DMF in the upper limit regions proceed quite rapidly. In fact the k_{CS} values are close to 10^{12} s^{-1}, which is close to the correlation times of solvent relaxation (0.5–1 ps). This might indicate the possibility that the CS rates at the upper limit region in these solvents are solvent controlled in the adiabatic regime or rather close to such situation.

Although the energy-gap dependencies of k_{CR} indicted in Figures 8b and 8c for THF and DMF seem to be reproduced approximately with Equation (10) assuming appropriate parameter values; they can be equally well or better reproduced by the linear (exponential) energy-gap law as indicated in Figure 9 from an unbiased viewpoint. It should be noted here

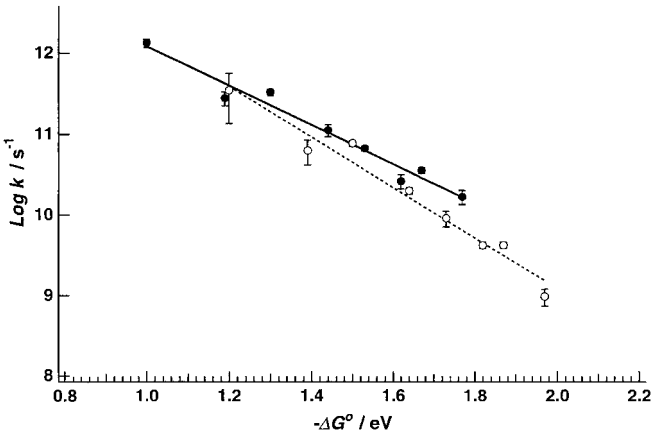

Figure 9. Logk_{CR} versus $-\Delta G_{CR}$ linear polts for THF (○) and DMF (●) solutions. The lines were calculated by the following equations: logk_{CR} = 15.5 – 3.12($-\Delta G_{CR}$) (- - - -) and logk_{CR} = 14.0 – 2.10($-\Delta G_{CR}$) (——).

that the nature of the ET in the so-called inverted region is fundamentally different from that in the normal region. The CR in the inverted region is conceptually analogous to the radiationless transition (internal conversion) in the weak coupling limit, because of the embedded nature of the potential surface of the initial state in that of the final state and because of the transition between different eigenstates of the same Hamiltonian, due to the coupling with promoting and accepting quantum modes of the intramolecular vibrations. Namely, the transition in the inverted region is greatly facilitated by the quantum-mechanical tunneling due to intrachromophore high-frequency modes. Such tunneling effects are not so important in the normal region owing to the different nature of the energy surfaces. Moreover, such a

0947-6539/00/0601-0042 $ 17.50+.50/0 *Chem. Eur. J.* **2000**, *6*, No. 1

quantum-tunneling mechanism may be more effective in the systems with stronger inter-chromophore electronic interactions, such as the CIPs described in the Introduction and linked systems with stronger inter-chromophore interactions like the present ZH dyad systems.

On the basis of the previous theoretical treatments of the radiationless transition in the weak coupling limit,[29] it is possible to give an approximate equation for the energy-gap dependency of k_{CR} in the inverted region [Eqs. (14a) and (14b)].[29, 30]

$$\ln k_{CR} = \ln C - (\gamma/\hbar\omega_M)\,|\,\Delta G_{CR}\,| \tag{14a}$$

$$\gamma = \ln(|\,\Delta G_{CR}\,|/S_M\hbar\omega_M) - 1 \tag{14b}$$

In Equations (14a) and (14b) $S_M = \sum_j S_j$, $\omega_M = \sum_j \omega_j S_j/S_M$, and $S_j = 1/2(M_j\omega_j/\hbar)(\Delta Q_j)^2$. The preexponential factor C represents mainly the contribution from the electronic-coupling term that connects the ET state with the ground state, and also some additional term.[30] The term $-(\gamma/\hbar\omega)\,|\,\Delta G_{CR}\,|$ arises from the energy release into acceptor modes during the CR transition. S_M and ω_M are average quantities for electron-vibrational coupling constants S_j and angular frequencies ω_M of the quantum modes, and S_j is given as a function of the equilibrium displacements ΔQ_j. Although γ contains ΔG_{CR}, its variation with change of ΔG_{CR} is much smaller than that of $\ln k_{CR}$. Thus, the linear energy-gap law in Figure 9 can be interpreted in the weak coupling limit of the intramolecular radiationless transition, in an analogous manner to the CR of CIPs produced by excitation of the ground state CT complexes.[7a,d,f,g, 15]

It should be noted here that the right hand side of Equation (14a) should contain the term due to the solvent reorganization because both intramolecular high-frequency and low-frequency modes of solvents surrounding or coordinated to solute are usually important for ET reaction. Nevertheless, the $\ln k_{CR}$ versus $-\Delta G_{CR}$ linear energy-gap law of CIP's was hardly affected by the change of the solvent polarity.[15d] This trend has been interpreted to indicate overwhelming effects of the high-frequency quantum modes on the CR reaction and only a minor contribution from the solvent modes owing to the plane parallel, rather tight structures of the CIPs. On the other hand, in the present ZH systems, we can recognize some solvent effects from different slopes of the $\log k_{CR}$ versus $-\Delta G_{CR}$ relationship between THF and DMF (Figure 9). This result might be ascribed to the more open structure of ZH systems which is more accessible for solvation or solvent coordination, although the detailed mechanisms for the solvent effects on the slope is not very clear at the present stage of the investigations. It should be noted here that, in the case of the porphyrin–quinone linked systems studied previously,[9a] measurements of the k_{CR} versus $-\Delta G_{CR}$ relationship in polar solvents were very limited and only some k_{CR} values were obtained for THF. Therefore, whether the energy-gap law for the CR of this porphyrin–quinone-linked system in polar solvents can be reproduced by the linear relationship or not is not very clear at present either.

Conclusions

In conclusion, we summarize here the main points of the present investigation and their significance for the further development of the related fields.

1) In spite of a fairly large energy gap for the CS reaction in polar solvents, no inverted regions were detected, but further trial is apparently necessary for its final clear-cut confirmation with distance-fixed chromophore systems.
2) The results of the simulations of the observed ET rate constants, including both k_{CS} and k_{CR}, over a wide energy-gap range, calculated with Equation (10), indicate that the nonadiabatic mechanism is still applicable. Estimated reorganization energies (0.62 eV in benzene, 0.82 eV in THF, and 0.84 eV in DMF) were certainly smaller than those of the previously studied porphyrin–quinone dyads and smaller than those of Gust and Moore's porphyrin dyads in CH_2Cl_2.[11] On the other hand, the k_{CS} values at the upper limit regions in THF and DMF are close to $10^{12}\ s^{-1}$, which is rather close to the correlation times of solvent relaxation in these aprotic polar solvents. These results seem to suggest that, owing to the strong inter-chromophore interactions, the CS rates here approaches that of the solvent-controlled one in adiabatic regime. With further fine control of the strength of inter-chromophore interactions responsible for ET in some elaborate linked chromophore systems, important information concerning the details of ET mechanisms will be obtained.
3) The energy-gap dependencies of k_{CR} in THF and DMF were reproduced approximately by Equation (10), but can be reproduced also well or better by the linear energy-gap law that was observed previously for the CR of CIPs (contact ion pair) with strong inter-ionic interactions. The non-Marcus type energy-gap laws of CIPs were shown to be insensitive to the change of solvent polarity, probably due to their plane-parallel sandwich structures, while we have confirmed here that the slope of $\log k_{CR}$ versus $-\Delta G_{CR}$ linear relationship in the ZH systems changes with solvent polarity. This result may be ascribed to more open structure of the ZH systems that is favorable for solvation. In order to elucidate the details of the mechanisms underlying the linear energy-gap law and its solvent dependencies, investigations on porphyrin dyad systems with variations in the inter-chromophore interactions and with different inter-chromophore configurations, which include plane-parallel sandwich structures, will be crucially important. Studies along in this line are actively in progress in our groups.

The investigations indicated above for the further elucidation of the fundamental mechanisms related to the present studies will be of crucial importance also for the construction of artificial photosynthetic systems and related devices.

Experimental Section

Unless otherwise stated, all commercially available regents and solvents were used without further purification. Acetonitrile and dichloromethane were refluxed over and distilled from P_2O_5. Preparative separations were

performed usually by flash column chromatography on silica gel (Merck, Kieselgel 60H; Art. 7736). ^{1}H NMR spectra were recorded on a JEOL α-500 spectrometer (operating as 500 MHz) and chemical shifts were represented as δ-values relative to the internal standard TMS. UV/Visible spectra were recorded on a Shimadzu UV-3000 spectrometer, and steady-state fluorescence spectra were taken on a RF-502A spectrofluorometer. Mass spectra were recorded on a JEOL HX-110 mass spectrometer with a 3-nitrobenzylalcohol matrix. Fluorescence lifetimes were measured on 10^{-7} M solutions with a picosecond time-correlated single-photon counting system.[31] Time-resolved transient absorption spectra were measured by using two laser systems. One was for the measurements in picosecond time region and the other was in subpicosecond time region. For the picosecond measurements, a dye laser (Rh-640) pumped by a second harmonic of a mode-locked Nd^{3+}:YAG laser (Quantel, Pico-chrome YG-503C/PTL – 10) was used as exciting light. A continuum probe pulse was made by focusing a fundamental of the Nd^{3+}:YAG laser into a quartz cell containg D_2O. The repetition of the laser pulse was 10 Hz and the signal was accumulated for 30 pulses. The solutions were excited at 630 nm and the free-base porphyrins were selectively excited to the S_1 states. The time resolution of the system was about 10 ps.[32] For the subpicosecond measurements, a synchronously pumped rhodamine 6G dye laser pumped by a second harmonic of a mode-locked CW Nd^{3+}:YAG laser (Quantronix, 82 Mhz) was used. The output of the dye laser was amplified by 4-stage dye amplifier excited by a regenerative YAG amplifier (Contiuum) with 50 Hz. The wavelength of a pump was 590 nm and the signal was accumulated for 50 pulses. The time resolution of the system was about 500 fs.[33] The measurements in the subpicosecond region were done for **5**–**8ZH** in THF and for **1**–**8ZH** in DMF. Concentrations of the solutions were about 2.0×10^{-4} M and all the solutions were deaerated by a nitrogen stream just prior to the measurements. The values of k_{CS} and k_{CR} were determined on the basis of the time profiles at several wavelengths and the errors were also estimated and are listed in Table 3.

General procedure for synthesis of 1–8ZH: The synthesis of **1ZH** is described here as a typical example. Aldehyde **1FH** (30 mg, 0.05 mmol), 2,6-dibenzyloxybenzaldehyde (**9**; 80 mg, 0.25 mmol) and di[3-hexyl-4-methyl(pyrrol-2-yl)]methane (**10**; 103 mg, 0.3 mmol) were dissolved in $CHCl_3$/CH_3CN (1:1; 50 mL). Trichloroacetic acid (100 mg) was added to the mixture, and the resulting solution was stirred for 16 h in the dark under nitrogen. *p*-Chloranil (110 mg, 0.45 mmol) was added, and the mixture was stirred for additional 8 h. The reaction mixture was poured into aqueous $NaHCO_3$ and extracted with CH_2Cl_2; the organic layer was separated and dried over Na_2SO_4, and the solvent was evaporated. The product was preliminary purified by being passed through a short alumina column with CH_2Cl_2, and the solvent was evaporated. Porphyrin dimer was separated by flash column chromatography over silica gel with $CHCl_3$ as a eluent. After evaporation of the solvent, the recrystallization from CH_2Cl_2/MeOH gave **1HH** (14 mg, 9 μmol, 18%, yield based on the amount of **1FH** used). Then, a solution of $Zn(OAc)_2$ (7.7 μmol) in MeOH (0.5 mL) was added to a solution of **1HH** (12 mg, 7.7 μmol) dissolved in CH_2Cl_2 (5 mL). The mixture was stirred for 5 min and diluted with water to effect preferential Zn^{II} insertion to the β-alkylated porphyrin. The organic layer was separated and dried over Na_2SO_4, and the solvent was evaporated. The monozinc product was separated by flash column chromatography with a mixture of $CHCl_3$/hexane as a eluent. After evaporation of the solvent, the recrystallization from CH_2Cl_2/MeOH gave **1ZH** (9 mg, 5 μmol, 75% yield based on the amount of **1HH** used). ^{1}H NMR ($CDCl_3$): $\delta = 10.45$ (s, 2H; *meso*), 10.29 (s, 2H; *meso*), 9.63 (d, $J = 4.4$ Hz, 2H; β-position), 9.55 (d, $J = 4.4$ Hz, 2H; β-position), 9.48 (d, $J = 4.9$ Hz, 2H; β-position), 9.20 (d, $J = 4.9$ Hz, 2H; β-position), 8.67 (d, $J = 7.8$ Hz, 2H; Ar-H), 8.57 (d, $J = 7.8$ Hz, 2H; Ar-H), 8.19 (d, $J = 1.5$ Hz, 2H; Ar-H), 7.87 (t, 1H; Ar-H), 7.64 (t, $J = 8.3$ Hz, 1H; Ar-H), 7.03 (d, $J = 8.3$ Hz, 2H; Ar-H), 6.83 (t, $J = 7.3$ Hz, 2H; Ar-H), 6.70 (t, $J = 7.6$ Hz, 4H; Ar-H), 6.58 (d, $J = 7.3$ Hz, 4H; Ar-H), 4.99 (s, 4H; benzyl-H), 4.18 (t, $J = 9.8$ Hz, 4H; hex-1), 4.05 (t, $J = 9.5$ Hz, 4H; hex-1), 3.18 (s, 6H; Me), 2.62 (s, 6H; Me), 2.36 (m, 4H; hex-2), 2.25 (m, 4H; hex-2), 1.90 (m, 4H; hex-3), 1.79 (m, 4H; hex-3), 1.61 (s, 18H; *t*Bu), 1.3–1.6 (m, 16H; hex-4,5), 0.98 (t, 6H; $J = 7.3$ Hz, hex-6), 0.92 (t, 6H; $J = 7.3$ Hz, hex-6), −2.8, −2.9 (br, 1H, 1H; NH); MS: *m*/*z*: 1625 calcd for $C_{108}H_{120}O_2N_8Zn$; found 1625.

Spectral data of 2–8ZH

Dyad 2ZH: ^{1}H NMR ($CDCl_3$): $\delta = 10.29$ (s, 1H; *meso*), 10.28 (s, 2H; *meso*), 9.99 (d, $J = 4.3$ Hz, 1H; β-position), 9.82 (d, $J = 4.9$ Hz, 1H; β-position), 9.50 (d, $J = 4.9$ Hz, 1H; β-position), 9.43 (dd, 2H; β-position), 9.36 (d, $J = 4.3$ Hz, 1H; β-position), 9.07 (d, $J = 4.9$ Hz, 1H; β-position), 9.06 (d, $J = 4.9$ Hz, 1H; β-position), 8.60 (d, $J = 7.3$ Hz, 2H; Ar-H), 8.54 (d, $J = 8.0$ Hz, 2H; Ar-H), 8.12 (d, $J = 1.5$ Hz, 2H; Ar-H), 7.86 (t, 1H; Ar-H), 7.64 (t, $J = 8.6$ Hz, 1H; Ar-H), 7.03 (d, $J = 8.6$ Hz, 2H; Ar-H), 6.82 (t, $J = 7.4$ Hz, 2H; Ar-H), 6.68 (t, $J = 7.3$ Hz, 4H; Ar-H), 6.56 (d, $J = 7.9$ Hz, 4H; Ar-H), 4.98 (s, 4H; benzyl-H), 4.18 (t, $J = 7.9$ Hz, 4H; hex-1), 4.03 (t, $J = 6.7$, 8.7 Hz, 4H; hex-1), 3.14 (s, 6H; Me), 2.61 (s, 6H; Me), 2.36 (m, 4H; hex-2), 2.26 (m, 4H; hex-2), 1.90 (m, 4H; hex-3), 1.79 (m, 4H; hex-3), 1.59 (s, 18H; *t*Bu), 1.3-1.6 (m, 16H; hex-4,5), 0.97 (t, $J = 7.4$ Hz, 6H; hex-6), 0.92 (t, $J = 7.4$ Hz, 6H; hex-6), −2.80 (br, 2H; NH); MS: *m*/*z*: 1706.6 calcd for $C_{108}H_{119}O_2N_8Br$; found 1702.79.

Dyad 3ZH: ^{1}H NMR ($CDCl_3$): $\delta = 10.48$ (s, 2H; *meso*), 10.29 (s, 2H; *meso*), 9.63 (d, $J = 4.3$ Hz, 2H; β-position), 9.57 (d, $J = 4.8$ Hz, 2H; β-position), 9.54 (d, $J = 4.3$ Hz, 2H; β-position), 9.03 (d, $J = 4.3$ Hz, 2H; β-position), 8.66 (d, $J = 7.9$ Hz, 2H; Ar-H), 8.58 (d, $J = 7.3$ Hz, 2H; Ar-H), 7.65 (t, $J = 8.5$ Hz, 1H; Ar-H), 7.04 (d, $J = 8.6$ Hz, 2H; Ar-H), 6.83 (t, $J = 7.4$ Hz, 2H; Ar-H), 6.69 (t, $J = 7.6$ Hz, 4H; Ar-H), 6.57 (d, $J = 7.4$ Hz, 4H; Ar-H), 4.99 (s, 4H; benzyl-H), 4.19 (t, $J = 7.7$ Hz, 4H; hex-1), 4.04 (t, $J = 7.4$ Hz, 4H; hex-1), 3.16 (s, 6H; Me), 2.62 (s, 6H; Me), 2.37 (m, 4H; hex-2), 2.26 (m, 4H; hex-2), 1.90 (m, 4H; hex-3), 1.80 (m, 4H; hex-3), 1.3–1.6 (m, 16H; hex-4,5), 0.98 (t, $J = 7.4$ Hz, 6H; hex-6), 0.93 (t, $J = 7.4$ Hz, 6H; hex-6), −2.92, −3.01 (br, 1H, 1H; NH); MS: *m*/*z*: 1603 calcd for $C_{100}H_{99}O_2N_8F_5Zn$; found 1603.

Dyad 4ZH: ^{1}H NMR ($CDCl_3$): δ 10.29 (s, 2H; *meso*), 9.87 (d, $J = 4.9$ Hz, 2H; β-position), 9.70 (d, $J = 4.9$ Hz, 2H; β-position), 9.35 (d, $J = 4.3$ Hz, 2H; β-position), 8.95 (d, $J = 4.4$ Hz, 2H; β-position), 8.56 (d, $J = 8.0$ Hz, 2H; Ar-H), 8.54 (d, $J = 8.0$ Hz, 2H; Ar-H), 8.07 (d, $J = 1.9$ Hz, 2H; Ar-H), 7.86 (t, 1H; Ar-H), 7.65 (t, $J = 8.6$ Hz, 1H; Ar-H), 7.04 (d, $J = 8.6$ Hz, 2H; Ar-H), 6.83 (t, $J = 8.0$ Hz, 2H; Ar-H), 6.69 (t, $J = 8.0$ Hz, 4H; Ar-H), 6.57 (d, $J = 7.3$ Hz, 4H; Ar-H), 4.99 (s, 4H; benzyl-H), 4.18 (t, $J = 7.0$ Hz, 4H; hex-1), 4.04 (t, $J = 9.7$ Hz, 4H; hex-1), 3.13 (s, 6H; Me), 2.61 (s, 6H; Me), 2.37 (m, 4H; hex-3), 2.25 (m, 4H; hex-2), 1.90 (m, 4H; hex-3), 1.80 (m, 4H; hex-3), 1.58 (s, 18H; *t*Bu), 1.3–1.6 (m, 16H; hex-4,5), 0.98 (t, $J = 7.3$ Hz, 6H; hex-6), 0.93 (t, $J = 7.3$ Hz, 6H; hex-6), −2.52 (br, 2H; NH); MS: *m*/*z*: 1788 calcd for $C_{108}H_{120}O_2N_8Br_2Zn$; found 1783.

Dyad 5ZH: ^{1}H NMR ($CDCl_3$): $\delta = 10.28$ (s, 2H; *meso*), 9.49 (d, $J = 4.5$ Hz, 2H; β-position), 9.09 (d, $J = 3.5$ Hz, 2H; β-position), 8.99 (d, $J = 4.0$ Hz, 2H; β-position), 8.95 (d, $J = 4.0$ Hz, 2H; β-position), 8.61 (d, $J = 7.5$ Hz, 2H; Ar-H), 8.56 (d, $J = 7.5$ Hz, 2H; Ar-H), 7.64 (t, $J = 8.8$ Hz, 1H; Ar-H), 7.03 (d, $J = 9.0$ Hz, 2H; Ar-H), 6.82 (t, $J = 7.5$ Hz, 2H; Ar-H), 6.69 (t, $J = 8.5$ Hz, 4H; Ar-H), 6.56 (d, $J = 7.0$ Hz, 4H; Ar-H), 4.98 (s, 4H; benzyl-H), 4.16 (t, $J = 7.5$ Hz, 4H; hex-1), 4.04 (t, $J = 7.5$ Hz, 4H; hex-1), 3.09 (s, 6H; Me), 2.61 (s, 6H; Me), 2.34 (m, 4H; hex-2), 2.25 (m, 4H; hex-2), 1.88 (m, 4H; hex-3), 1.79 (m, 4H; hex-3), 1.3–1.6 (m, 16H; hex-4,5), 0.97 (t, $J = 7.3$ Hz, 6H; hex-6), 0.92 (t, $J = 7.3$ Hz, 6H; hex-6), −2.66 (s, 2H; NH): MS: *m*/*z*: 1935 calcd for $C_{112}H_{97}O_2N_8F_{15}Zn$; found 1935.

Dyad 6ZH: ^{1}H NMR ($CDCl_3$): $\delta = 10.38$ (s, 1H; *meso*), 10.27 (s, 1H; *meso*), 10.26 (s, 1H; *meso*), 9.58 (d, $J = 5.0$ Hz, 1H; β-position), 9.53 (d, $J = 5.0$ Hz, 1H; β-position), 9.49 (d, $J = 5.0$ Hz, 1H; β-position), 9.48 (d, $J = 4.0$ Hz, 1H; β-position), 9.46 (d, $J = 4.5$ Hz, 1H; β-position), 9.42 (d, $J = 4.0$ Hz, 1H; β-position), 9.03 (d, $J = 5.0$ Hz, 1H; β-position),8.96 (d, $J = 4.0$ Hz, 1H; β-position), 8.56 (br, 4H; Ar-H), 7.65 (t, $J = 8.8$ Hz, 1H; Ar-H), 7.04 (d, $J = 9.0$ Hz, 2H; Ar-H), 6.81 (t, $J = 7.5$ Hz, 2H; Ar-H), 6.69 (t, $J = 7.8$ Hz, 4H; Ar-H), 6.57 (d, $J = 8.0$ Hz, 4H; Ar-H), 4.99 (s, 4H; benzyl-H), 4.14 (t, $J = 9.5$ Hz, 4H; hex-1), 4.03 (t, $J = 7.8$ Hz, 4H; hex-1), 3.10 (s, 3H; Me), 3.09 (s, 3H; Me), 2.62 (s, 6H; Me), 2.34 (m, 4H; hex-2), 2.25 (m, 4H; hex-2), 1.87 (m, 4H; hex-3), 1.79 (m, 4H; hex-3), 1.3–1.6 (m, 16H; hex-4,5), 0.9–1.0 (m, 12H; hex-6), −2.91 (s, 2H; NH); MS: *m*/*z*: 1647 calcd for $C_{100}H_{98}O_9N_9F_5Zn$; found 1648.

Dyad 7ZH: ^{1}H NMR ($CDCl_3$): $\delta = 10.29$ (s, 2H; *meso*), 9.75 (br, 2H; β-position), 9.64 (br, 2H; β-position), 9.50 (d, $J = 5.0$ Hz, 2H; β-position), 8.95 (d, $J = 5.0$ Hz, 2H; β-position), 8.56 (dd, 4H; Ar-H), 7.64 (t, $J = 8.5$ Hz, 1H; Ar-H), 7.03 (d, $J = 9.0$ Hz, 2H; Ar-H), 6.82 (t, $J = 8.0$ Hz, 2H; Ar-H), 6.69 (t, $J = 7.5$ Hz, 4H; Ar-H), 6.56 (d, $J = 7.0$ Hz, 4H; Ar-H), 4.98 (s, 4H; benzyl-H), 4.19 (t, $J = 7.5$ Hz, 4H; hex-1), 4.03 (t, $J = 7.5$ Hz, 4H; hex-1), 3.16 (s, 6H; Me), 2.60 (s, 6H; Me), 2.36 (m, 4H; hex-2), 2.34 (m, 4H; hex-2), 1.90 (m, 4H; hex-3), 1.79 (m, 4H; hex-3), 1.3–1.6 (m, 16H; hex-4,5), 0.97 (t, $J = 7.5$ Hz, 6H; hex-6), 0.92 (t, $J = 7.3$ Hz, 6H; hex-6), −2.38 (s, 2H; NH); MS: *m*/*z*: 1940 calcd for $C_{106}H_{97}O_2N_8F_{19}Zn$; found 1939.

0947-6539/00/0601-0044 $ 17.50+.50/0 *Chem. Eur. J.* **2000**, *6*, No. 1

Dyad 8ZH: ^{1}H NMR ($CDCl_3$): $\delta = 10.27$ (s, 2H; *meso*), 9.54 (d, $J = 5.0$ Hz, 2H; β-position), 9.50 (d, $J = 5.0$ Hz, 2H; β-position), 9.45 (d, $J = 5.0$ Hz, 2H; β-position), 8.98 (d, $J = 4.5$ Hz, 2H; β-position), 8.60 (d, $J = 7.5$ Hz, 2H; Ar-H), 8.56 (d, $J = 8.0$ Hz, 2H; Ar-H), 7.64 (t, $J = 8.5$ Hz, 1H; Ar-H), 7.03 (d, $J = 8.5$ Hz, 2H; Ar-H), 6.80 (t, $J = 7.5$ Hz, 2H; Ar-H), 6.67 (t, $J = 7.5$ Hz, 4H; Ar-H), 6.55 (d, $J = 8.5$ Hz, 4H; Ar-H), 4.97 (s, 4H; benzyl-H), 4.16 (t, $J = 7.5$ Hz, 4H; hex-1), 4.02 (t, $J = 7.5$ Hz, 4H; hex-1), 3.08 (s, 6H; Me), 2.60 (s, 6H; Me), 2.34 (m, 4H; hex-2), 2.23 (m, 4H; hex-2), 1.88 (m, 4H; hex-3), 1.78 (m, 4H; hex-3), 1.3–1.6 (m, 16H; hex-4,5), 0.96 (t, $J = 7.5$ Hz, 6H; hex-6), 0.91 (t, $J = 7.5$ Hz, 6H; hex-6), −2.86 (br, 2H; NH); MS: *m*/*z*: 1697 calcd for $C_{100}H_{97}O_6N_{10}F_5Zn$; found 1693.

Acknowledgments

This work was partly supported by Grant-in-Aid of Scientific Research from the Ministry of Education, Science, Sports, and Culture of Japan.

[1] R. A. Marcus, *J. Chem. Phys.* **1956**, *24*, 966.
[2] R. A. Marcus, N. Sutin, *Biochim. Biophys. Acta* **1985**, *811*, 265.
[3] a) C. Kirmaier, D. Holten, *Photosynth. Res.* **1987**, *13*, 225; b) N. W. Woodbury, J. P. Allen, in *Anoxugenic Photosynthetic Bacteria* (Eds.: R. E. Blankenship, M. T. Madigan, C. E. Bauer), Kluwer Academic, Dordecht, **1994**, chapter 24, p. 527, and references cited therein.
[4] a) M. R. Wasielewski, *Chem. Rev.* **1992**, *92*, 435; b) G. L. Closs, J. R. Miller, *Science* **1988**, *240*, 440; c) D. Gust, T. A. Moore, A. L. Moore, *Acc. Chem. Res.* **1993**, *26*, 198; d) H. Kurreck, M. Huber, *Angew. Chem.* **1995**, *107*, 929; *Angew. Chem. Int. Ed. Engl.* **1995**, *34*, 849; e) K. Maruyama, A. Osuka, N. Mataga, *Pure Appl. Chem.* **1994**, *66*, 867; f) A. Osuka, N. Mataga, T. Okada, *Pure Appl. Chem.* **1997**, *69*, 797; g) "Photoprocesses in Transition Metal Complexes, Biosystems and Other Molecules", J. W. Verhoeven, M. N. Paddon-Row, J. W. Warman, *NATO ASI Ser.* **1989**, *376*, 271.
[5] a) M. R. Gunner, D. E. Robertson, P. L. Dutton, *J. Phys. Chem.* **1986**, *90*, 3783; b) M. R. Gunner, P. L. Dutton, *J. Am. Chem. Soc.* **1989**, *111*, 3400; c) M. Iwaki, S. Kumazaki, K. Yoshihara, T. Erabi, S. Ito, *J. Phys. Chem.* **1996**, *100*, 10802.
[6] a) J. R. Miller, L. T. Calcaterra, G. L. Closs, *J. Am. Chem. Soc.* **1984**, *106*, 3047; b) J. R. Miller, J. V. Beitz, R. K. Huddleston, *J. Am. Chem. Soc.* **1984**, *106*, 5057.
[7] a) "Electron Transfer in Inorganic, Organic, and Biological Systems", N. Mataga, *Adv. Chem. Ser.* **1991**, *228*, 91; b) "Electron Transfer in Inorganic, Organic, and Biological Systems", T. Kakitani, A. Yoshimori, N. Mataga, *Adv. Chem. Ser.* **1991**, *228*, 45; c) N. Mataga, *Pure Appl. Chem.* **1993**, *65*, 1605; d) N. Mataga, H. Miyasaka, *Prog. React. Kinet.* **1994**, *19*, 317; e) T. Kakitani, N. Matsuda, A. Yoshimori, N. Mataga, *Prog. React. Kinet.* **1995**, *20*, 347; f) N. Mataga, *Pure Appl. Chem.* **1997**, *69*, 729; g) "Electron Transfer: From Isolated Molecules to Biomolecules", N. Mataga, H. Miyasaka, *Adv. Chem. Phys.* **1998**, *107*, 431.
[8] a) M. R. Wasielewski, M. P. Niemczyk, W. A. Svec, E. B. Pewitt, *J. Am. Chem. Soc.* **1985**, *107*, 1080; b) "Supramolecular Photochemistry", M. R. Wasielewski, D. G. Johnson, W. A. Svec, *NATO ASI Ser.* **1987**, *214*, 255; c) G. L. Gaines III, M. P. O'Neil, W. A. Svec, M. P. Niemczyk, M. R. Wasielewski, *J. Am. Chem. Soc.* **1991**, *113*, 719; d) R. J. Harrison, B. Pearce, G. S. Beddard, J. A. Cowan, J. K. M. Sanders, *Chem. Phys.* **1987**, *116*, 429; e) N. Mataga, A. Karen, T. Okada, S. Nishitani, N. Kurata, Y. Sakata, S. Misumi, *J. Phys. Chem.* **1984**, *88*, 5138.
[9] a) T. Asahi, M. Ohkohchi, R. Matsusaka, N. Mataga, R. P. Zhang, A. Osuka, K. Maruyama, *J. Am. Chem. Soc.* **1993**, *115*, 5665; b) A. Osuka, R. P. Zhang, K. Maruyama, I. Yamazaki, Y. Nishimura, *Bull. Chem. Soc. Jpn.* **1992**, *65*, 2807.
[10] a) H. Heitele, F. Pöllinger, T. Häberle, M. E. Michel-Beyerle, H. A. Staab, *J. Phys. Chem.* **1994**, *98*, 7402; b) A. D. Joran, B. A. Leland, P. M. Felker, A. H. Zweil, J. J. Hopfield, P. B. Dervan, *Nature* **1987**, *107*, 1080.
[11] a) D. Gust, T. A. Moore, A. L. Moore, L. Leggett, S. Lin, J. M. DeGraziano, R. M. Hermant, DF. Nicodem, P. Craig, G. R. Seely, R. Nieman, *J. Phys. Chem.* **1993**, *97*, 7926; b) J. M. DeGraziano, P. A. Liddell, L. Leggett, A. L. Moore, T. A. Moore, D. Gust, *J. Phys. Chem.* **1994**, *98*, 1758. c) J. M. DeGraziano, A. N. Macpherson, P. A. Liddell, L. Noss, J. P. Sumida, G. R. Seely, J. E. Lewis, A. L. Moore, T. A. Moore, D. Gust, *New. J. Chem.* **1996**, *20*, 839.
[12] Observation of the moderately inverted region has been reported for the photoinduced CS of covalently linked porphyrin–quinones on the kinetic results obtained by the fluorescence upconversion method and sub-picosecond transient absorption methods. a) T. Häberle, J. Hirsch, F. Pöllinger, H. Heitele, M. E. Michel-Beyerle, C. Anders, A. Döhlling, C. Krieger, A. Rückemann, H. A. Staab, *J. Phys. Chem.* **1996**, *100*, 18269; b) F. Pöllinger, C. Musewald, H. Heitele, M. E. Michel-Beyerle, C. Anders, M. Futscher, G. Voit, H. A. Staab, *Ber. Bunsenges. Phys. Chem.* **1996**, *100*, 207.
[13] a) T. Ohno, A. Yoshimura, N. Mataga, *J. Phys. Chem.* **1986**, *90*, 3295; b) N. Mataga, Y. Kanda, T. Okada, *J. Phys. Chem.* **1986**, *90*, 3880; c) T. Ohno, A. Yoshimura, N. Mataga, S. Tazuke, Y. Kawanishi, *J. Phys. Chem.* **1989**, *93*, 3546; d) N. Mataga, T. Asahi, Y. Kanda, T. Okada, T. Kakitani, *Chem. Phys.* **1988**, *127*, 249.
[14] I. R. Gould, S. Farid, *Acc. Chem. Res.* **1996**, *29*, 522.
[15] a) T. Asahi, N. Mataga, *J. Phys. Chem.* **1989**, *93*, 6575; b) T. Asahi, N. Mataga, Y. Takahashi, T. Miyashi, *Chem. Phys. Lett.* **1990**, *171*, 309; c) T. Asahi, N. Mataga, *J. Phys. Chem.* **1991**, *95*, 1956: d) T. Asahi, M. Ohkohchi, M. Nataga, *J. Phys. Chem.* **1993**, *97*, 13132; e) H. Miyasaka, S. Kotani, A. Itaya, G. Schweitzer, F. C. DeSchryver, N. Mataga, *J. Phys. Chem.* **1997**, *101*, 7978.
[16] a) D. Rehm, A. Weller, *Isr. J. Chem.* **1970**, *7*, 259; b) N. Mataga, Y. Kanda, T. Asahi, H. Miyasaka, T. Okada, T. Kakitani, *Chem. Phys.* **1988**, *127*, 239; c) A. Yoshimori, T. Kakitani, Y. Enomoto, N. Mataga, *J. Phys. Chem.* **1989**, *93*, 8316; d) S. Nishikawa, T. Asahi, T. Okada, T. Mataga, T. Kakitani, *Chem. Phys. Lett.* **1991**, *185*, 237; e) T. Kakitani, A. Yoshimori, N. Mataga, *J. Phys. Chem.* **1992**, *96*, 5385; f) N. Matsuda, T. Kakitani, T. Denda, N. Mataga, *Chem. Phys.* **1995**, *190*, 83.
[17] Although the plots were limited, detection of the inverted region in the intermolecular ET reaction of Ru^{II} diimide/Fe^{II} cytochrome *c* couple was reported recently. C. Turró, J. M. Zaleski, Y. M. Karabatson, D. G. Nocera, *J. Am. Chem. Soc.* **1996**, *118*, 6060.
[18] T. Nagata, *Bull. Chem. Soc. Jpn.* **1991**, *64*, 3005.
[19] T. Nagata, A. Osuka, K. Maruyama, *J. Am. Chem. Soc.* **1990**, *112*, 3054.
[20] a) J. S. Lindesy, I. C. Schreiman, H. C. Hsu, P. C. Kearney, A. M. Marguerettaz, *J. Org. Chem.* **1987**, *52*, 827; b) J. L. Sessler, V. L. Capuano, *Angew. Chem.* **1990**, *102*, 1162; *Angew. Chem. Int. Ed. Engl.* **1990**, *29*, 1134.
[21] S. G. DiMagno, V. S.-Y. Lin, M. J. Therien, *J. Org. Chem.* **1993**, *58*, 5983.
[22] a) J. E. Baldwin, M. J. Crossley, J. DeBernardis, *Tetrahedron* **1982**, *38*, 685; b) A. Osuka, H. Shimidzu, *Angew. Chem.* **1997**, *109*, 93; *Angew. Chem. Int. Ed. Engl.* **1997**, *36*, 135.
[23] K. M. Smith, G. H. Barnett, B. Evans, Z. Martynenko, *J. Am. Chem. Soc.* **1979**, *101*, 5953.
[24] C. H. Lee, J. S. Lindesy, *Tetrahedron* **1994**, *50*, 11427.
[25] a) J. A. Anton, P. A. Loach, Govindjee, *Photochem. Photobiol.* **1978**, *28*, 235; b) R. L. Brookfield, H. Ellul, A. Harriman, G. Porter, *J. Chem. Soc. Faraday Trans. 2* **1986**, *82*, 219; c) A. Osuka, K. Maruyama, I. Yamazaki, N. Tamai, *Chem. Phys. Lett.* **1990**, *165*, 392; d) J.-P. Strachan, S. Gentemann, J. Seth, W. A. Kalsbeck, J. S. Lindsey, D. Holten, D. F. Bocian, *J. Am. Chem. Soc* **1997**, *119*, 11191.
[26] a) A. Osuka, S. Marumo, K. Maruyama, N. Mataga, Y. Tanaka, S. Taniguchi, T. Okada, I. Yamazaki, Y. Nishimura, *Bull. Chem. Soc. Jpn.* **1995**, *68*, 262; b) A. Osuka, S. Marumo, N. Mataga, S. Taniguchi, T. Okada, I. Yamazaki, Y. Nishimura, T. Ohno, K. Nozaki, *J. Am. Chem. Soc.* **1996**, *118*, 155; c) S. Shinoda, H. Tsukube, Y. Nishimura, I. Yamazaki, A. Osuka, *Tetrahedron* **1997**, *53*, 13657.
[27] B. C. Perung, M. D. Newton, F. O. Raineri, H. L. Friedman, *J. Chem. Phys.* **1996**, *104*, 7153; B. C. Perung, M. D. Newton, F. O. Raineri, H. L. Friedman, *J. Chem. Phys.* **1996**, *104*, 7177.
[28] See for example: "Electron Transfer in Inorganic, Organic and Biological Systems", J. R. Bolton, M. D. Archer, *Adv. Chem. Ser.* **1991**, *228*, 7.
[29] a) R. Englman, J. Jortner, *Mol. Phys.* **1970**, *18*, 145; b) K. F. Freed, J. Jortner, *J. Chem. Phys.* **1970**, *52*, 6272.

[30] a) T. J. Meyer, *Prog. Inorg. Chem.* **1983**, *30*, 389; b) P. Chen, R. Duesing, G. Tapolsky, T. J. Meyer, *J. Am. Chem. Soc.* **1989**, *111*, 8305; c) P. Chen, R. Duesing, D. K. Graff, T. J. Meyer, *J. Phys. Chem*. **1991**, *95*, 5850.
[31] I. Yamazaki, N. Tamai, H. Kume, T. Tsuchiya, K. Oba, *Rev. Sci. Instrum.* **1985**, *56*, 1187.
[32] Y. Hirata, N. Mataga, *J. Phys. Chem.* **1991**, *95*, 1640.
[33] K. Nishiyama, Y. Asano, H. Hashimoto, T. Okada, *J. Mol. Liq.* **1995.** *65/66*, 41.

Received: March 22, 1999 [F1688]

0947-6539/00/0601-0046 $ 17.50+.50/0